Analysis and Transmitter Currents Decomposition Based Control for Multiple Overlapped Transmitters Based WPT Systems Considering Cross Couplings

Yong Li, *Student Member, IEEE*, Ruikun Mai, *Member, IEEE*, Liwen Lu, Tianren Lin, Yeran Liu, *Student Member, IEEE*, and Zhengyou He, *Senior Member, IEEE*

***Abstract*—Multiple transmitters powering a single receiver simultaneously is a good alternative to upgrade the power capacity of the wireless power transfer (WPT) system by using multiple modular inverters manufactured in a larger quantities, since the demand for high power applications is on the rise. A multiple overlapped transmitters based WPT system is presented in this paper. In order to alleviate the effects of the cross couplings between the transmitters, additional capacitors are adopted in the transmitters and the configuration of additional capacitors is provided. Virtual active and reactive powers are defined to decompose the transmitter current into active and reactive components. A transmitter current control scheme based on the proposed current decomposition method consisting of one reactive current control loop and one active current control loop is also presented in this paper. Finally, a low-scale experimental setup using two overlapped transmitters WPT system is provided to verify the proposed approach. The experimental results indicate that the proposed method could improve the stability of output voltage control and achieve minimal current difference amongst transmitters. Besides, the overall system efficiency is improved to 90.34% with the proposed control method at 1.45 kW output power, which demonstrates that the proposed method is a potential solution for high power applications.**

***Index Terms*—Active and reactive currents decomposition, multiple transmitters, output voltage regulation, wireless power transfer (WPT).**

Manuscript received October 8, 2016; revised December 31, 2016 and February 20, 2017; accepted March 26, 2017. Date of publication March 30, 2017; date of current version November 2, 2017. This work was supported in part by the National Natural Science Foundation of China under Grant 51507147, in part by the National Natural Science Foundation of China under Grant 51677155, in part by the National Science Fund for Distinguished Young Scholars under Grant 51525702, in part by the 2016 Doctoral Innovation Funds of Southwest Jiaotong University, and in part by the Scientific Talent Engineering Breeding Project of Sichuan Province under Grant 2016117. Recommended for publication by Associate Editor Prof. Chun T. Rim. *(Corresponding author: Zhengyou He.)*

Y. Li, R. Mai, T. Lin, Y. Liu, and Z. He are with the School of Electrical Engineering, Southwest Jiaotong University, Chengdu 610031, China (e-mail: leeo1864@163.com; mairk@swjtu.edu.cn; 445954204@qq.com; yeranliu@my.swjtu.edu.cn; hezy@swjtu.edu.cn).

L. Lu is with the School of Electrical Engineering, Southwest Jiaotong University, Chengdu 610031, China, and also with NR Electric Co. Ltd., Nanjing 211100, China (e-mail: 953390550@qq.com).

Color versions of one or more of the figures in this paper are available online at http://ieeexplore.ieee.org.

Digital Object Identifier 10.1109/TPEL.2017.2690061

I. Introduction

WIRELESS power transfer (WPT) is an emerging technology to deliver power from power source in the primary side to a load in the secondary side through magnetic coupling via a considerable air gap [1]–[6]. Recently, WPT has been extensively applied in various applications including wireless charging of biomedical implants [7], [8], mining applications [9], under-water power supply [10], and electric vehicles [11]–[20] due to its advantages of, e.g., convenience, safety, reliability, and immunity to ice, water, and other chemicals.

A. Current Problems

Generally, a high-frequency resonant inverter is adopted to feed the primary coil (also named transmitter), and the induced voltage of the secondary coil (also named receiver) in close proximity to the transmitter is generated by capturing magnetic flux around the transmitter. A conventional WPT system consists of a single transmitter and a single receiver. However, the power capacity of a single resonant inverter feeding the transmitter is limited by the constraints of semiconductor devices, and the single power supply results in a low reliability of the WPT system. This power supply (single resonant inverter) for WPT systems unlikely meets the requirement of high power applications since public transport systems need to be rated at hundreds of kVA or more (the required power to supply a high speed train is up to MW scale) [21]. However, contrary to the needs of a large capacity of power reaching to hundreds of kW and MW, the study of high-power WPT systems has not been paid much attention [22]. As a possible solution, high voltage, high current, and high frequency semiconductor devices are used to implement a high power transfer; unfortunately, these semiconductor devices are relatively expensive and may not be easy to purchase in the commercial market [22].

B. Literature Review

To address this problem, various approaches have been proposed to enhance the transmitted power of WPT systems by using low-power and low-cost semiconductor devices for high power application, e.g., railway transport [23]–[28]. One of them is to use a high-frequency multilevel inverter to supply WPT systems due to its advantages in terms of reducing the voltage

stress of semiconductor devices and increasing the output power capacity [23]–[25]. Harmonic distortion, power losses, and efficiency of multilevel inverter based WPT system were analyzed in detail by [23] and [24], and a cascaded multilevel converter for bidirectional IPT systems is presented in [25]. However, the cascaded structure of the multilevel inverter dramatically decreases the reliability of WPT systems.

Another approach is to use a multi-inverter connected in parallel to provide an amount of high-frequency current to the transmitter of WPT systems [26]. It proposes a parallel topology for WPT systems, which can achieve high output power levels in a cost-effective manner. However, large circulating currents among inverter modules generated by the component tolerance and other uncertainties increase extra power losses. In fact, some papers have proposed the configuration of a single inverter with multiple parallel MOSFETs to achieve a higher output current than that with a single MOSFET [29]–[32]. The parallel connection of MOSFETs can hand higher currents than a single MOSFET. Therefore, this configuration is widely employed in high power applications such as traction drives. The MOSFETs in parallel is an acceptable approach for reducing the size of the inverter and simplifying the structure of the circuit, and also a good alternative for the high power capability WPT system application. Although the MOSFETs are operated in parallel, once a fault occurs in one of the parallel MOSFETs, e.g., a short-circuit fault, the system will shut down. With the increasing of the number of parallel MOSFETs for each arm, it will be a great challenge to design a single gate driver to drive all the MOSFETs simultaneously and to develop a well-operated dissipation system for the inverter. In addition, compared to the parallel inverters with one MOSFET for each arm [33], [34], it does not own the characteristics of a high reliability, a good flexibility, and a convenient power extension. Both of the parallel connection methods mentioned above only adopt one transmitting coil in this system which results in only one energy transmission path between the transmitter and receiver. Once a fault occurs in the transmitter, the whole WPT system will not be in operation.

A 1 MW WPT system that supplies the power for a high speed train is proposed [21]. A total of five 200 kW inverter modules using insulated gate bipolar transistor (IGBT) switching elements are connected in series with the help of matching transformers feeding one transmitter to realize 1 MW. The inverters and matching transformers provide the energy to the transmitter with series connection. Therefore, if one inverter module or matching transformer has some faults, the whole system will break down. The reliability of the system is limited.

Some approaches using multiple transmitters to power a single receiver have been investigated in [27] and [28]. There is an increase in gain of the transmitted power due to the increased number of transmitters. Each of the independent transmitters can transfer power to the receiver. Thus, the number of energy transmission path is increased to N which depends on the number of the transmitters. One transmitter is fed by one inverter independently. Even if a fault occurs in one energy transmission path, the other energy transmission path still works normally. As a result, the reliability can be enhanced with this characteristic.

In order to improve the receive voltage, a practical power line synchronization technique is proposed to synchronize all transmitters [27]. Magnetic coupling among the transmitters is non-negligible when the transmitters are located close to each other. The effects of coupling among the multiple transmitters are discussed in [28]. The resonant frequencies are changed due to the magnetic coupling among the transmitters, which dramatically decrease the transfer efficiency. A frequency adjustment approach is proposed to improve the transfer efficiency. Unfortunately, the control of the output voltage and reliability of the WPT system were not paid enough attention by the aforementioned approaches.

C. Contributions

The main goal is to utilize multiple overlapped transmitters to enhance the transmitted power and increase the reliability of WPT systems. The proposed WPT system consists of two or more transmitters, and each transmitter is equipped with a resonant inverter unit. The resonant inverter units can be designed and manufactured in larger quantities to reduce the manufacturing cost, because redesigning and manufacturing a power supply is usually a time-consuming and expensive process. The work presented in this paper lays claim to the contributions as follows:

1) we demonstrate a WPT system based on multiple overlapped transmitters to enhance the transmitted power;
2) additional capacitors are adopted in the transmitters to mitigate/ eliminate the induced voltage caused by the cross coupling mutual inductance among the transmitters;
3) a transmitter current control scheme based on virtual active and reactive current decomposition is presented in this paper to suppress the current differences among transmitters, and the output voltage of the WPT system can also be regulated;
4) the reliability of the proposed WPT system is dramatically improved by the proposed control method and the overlapped structure.

II. Circuit Topology and Working Principle

A. System Configuration

Fig. 1 shows the configuration and the flux distribution of the WPT system based on two transmitters as an example without loss of generality, where the transmitters are totally overlapped and located close to each other. In order to enhance the coupling between the transmitter side and the receiver side, all the transmitters and receiver are wound around U-type ferrite cores as [21] did, which is a good alternative for railway applications. The proposed WPT system can be used for electric railway transportation applications, which need a large amount of power and a high reliability. It is worth noticing that the ferrite cores can be any other types, e.g., E-type, and/or I-type for various applications.

As shown from Fig. 2, a finite-element analysis software Flux is adopted to analyze and simulate the magnetic field of the dual transmitters based WPT system. It is clear that the magnetic field intensity of 10 A for a single transmitter (10 turns) is half that of 10 A for each of the dual transmitters (10 turns for each transmitter) due to the parallel overlapped structure. Therefore,

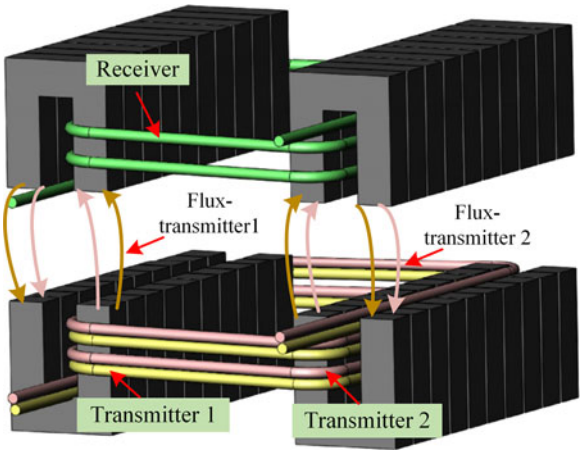

Fig. 1. Structure and flux distribution of the proposed WPT system.

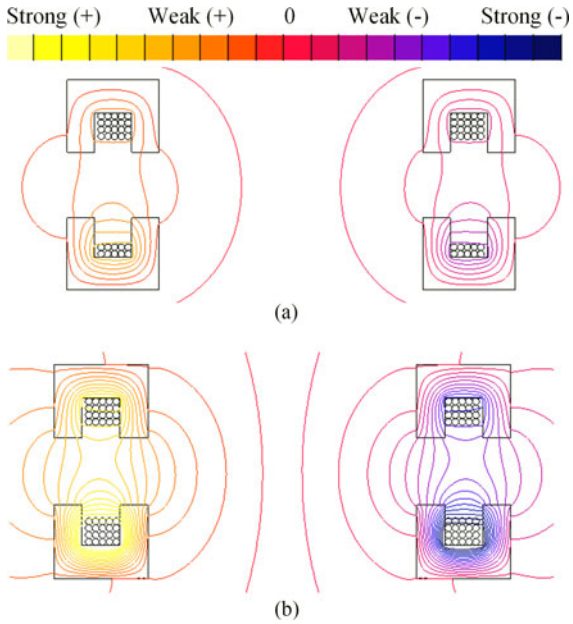

Fig. 2. Magnetic field image of the single transmitter and dual transmitters structure with different energized currents.

the magnetic field intensity can be enhanced by using multiple transmitters. Consequently, the WPT system based on multiple overlapped transmitters can meet the requirements of some high-power applications owing to the enhanced magnetic field.

It should be emphasized here that two 10-turn coils and one 20-turn coil can produce the same magnetic field for the same given coil current. However, the voltage of the 20-turn coil is much higher than that of the 10-turn coil due the larger self-inductance, which will lead to overvoltage problem. Moreover, one transmitter based WPT system suffers a low reliability. Once a fault occurs in the single transmitter coil or the inverter, the transmission of energy will be interrupted.

B. Operating Principle of the Proposed WPT System

The main circuit of the proposed WPT system is shown in Fig. 3, and each transmitter is equipped with a resonant inverter. The resonant inverter provides a high-frequency current to the

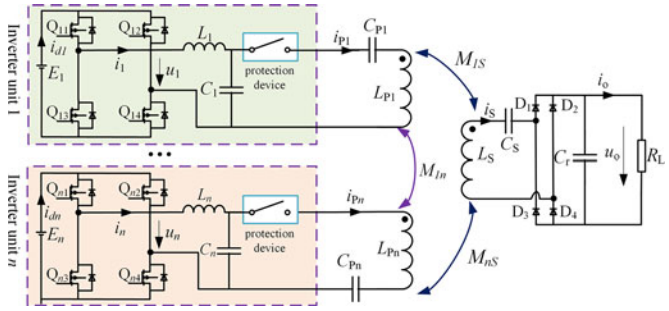

Fig. 3. Circuit configuration of the *LCL*-S tuned WPT system based on multiple transmitters.

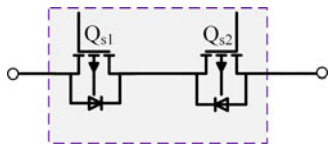

Fig. 4. Schematic of protection device.

corresponding transmitter. The series resonant compensation is employed in the secondary side to achieve constant output voltage. An *LCL* compensating network is adopted for each resonant inverter in the primary side due to its advantages [36]:

1) the inverter only supplies the active power required by the load without any reactive power when network is completely tuned;
2) the current in the transmitter is independent of the load, which makes it is easy to achieve constant transmitter current control.

$L_{p1} - L_{pn}$ are self-inductances of the transmitters, and the mutual inductances between the transmitters and receiver are M_{1s}–M_{ns}. Since the transmitters are identically wounded around the ferrite cores with the same shape and turns, the mutual inductances ($M_{1s} - M_{ns}$) are approximately equal to each other, $M_{1s} = \ldots = M_{ns} = M$. A bidirectional switch [35] is used as the protection device connected to the transmitter as shown in Fig. 4. The function of the bidirectional switch is to disconnect the faulty unit from the whole WPT system. Without the protection device, the WPT system may be out of service under faulty condition.

According to [36], the equivalent self-inductance of the transmitter become $L'_{pn} = L_{pn} - \frac{1}{\omega^2 C_{pn}}$ correspondingly. The inductance of L'_{pn} can be regulated by configuring C_{pn}. In order to tune the *LCL* network in the primary side and the series network in the secondary side to a constant resonant frequency, the circuit parameters are usually designed by the following equation [36]:

$$\omega = \frac{1}{\sqrt{L_n C_n}} = \frac{1}{\sqrt{L'_{\mathrm{pn}} C_n}} = \frac{1}{\sqrt{L_S C_S}}. \tag{1}$$

According to [37], the equivalent load R_0 of the rectified tank connected to a resistive load R_L can be expressed by

$$R_o = \frac{8R_L}{\pi^2}. \tag{2}$$

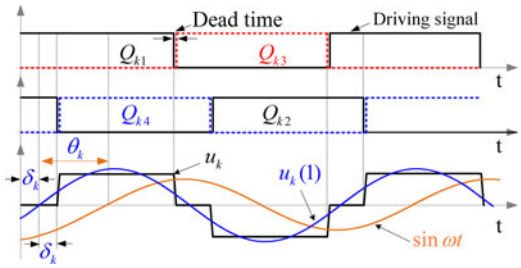

Fig. 5. Relevant voltage operating waveforms for PS-PWM.

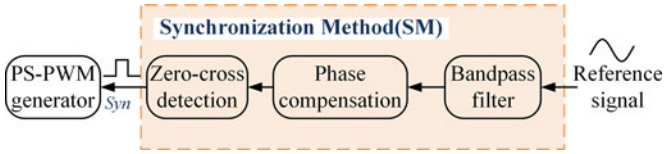

Fig. 6. Generation of the synchronization signal for the PS-PWM generator.

The output voltage of the inverter is controlled by the phase-shifted pulse width modulation (PS-PWM), and the voltage waveform is shown in Fig. 5. Alternatively, the fundamental output voltage of the kth inverter can be expressed as

$$u_k(t) = \frac{4E_k}{\pi}\cos\delta_k \sin(\omega t + \theta_k) \tag{3}$$

where E_k is the dc-link voltage and δ_k is half of the phase-shift angle between the two legs of the inverter, and θ_k is the angle between the output voltage and the reference signal $\sin(\omega t)$. By regulating δ_k and θ_k, it is possible to control both the amplitude and phase angle of the output voltage. As a result, the output voltage of each inverter can be regulated independently of other inverter units.

The synchronization reference signal which is used for the PS-PWM generator of the digital signal processor (DSP, TMS320F28335) controller is generated by the synchronization method (SM) as shown in Fig. 6. The reference signal passes through a band-pass filter to eliminate the harmonic components. A phase compensation circuit is applied to correct the phase error between the reference signal and synchronization signal caused by the filter. After that, a zero-cross detection circuit generates the square wave to the synchronization input port of the DSP. Then, the PS-PWM generator of the DSP controller can regulate δ_k and θ_k directly.

The fundamental voltage phasor of the kth inverter can be expressed as

$$\dot{U}_k = \frac{4E_k}{\pi}\cos\,\delta_k\,\cos\,\theta_k + j\frac{4E_k}{\pi}\,\cos\,\delta_k\,\sin\,\theta_k \tag{4}$$

where $\dot{U}_k$ represents the phasor form of $u_k(t)$.

C. Effects of the Cross Couplings in the Proposed WPT System and the Solution

It should be emphasized here that there is a relative large cross coupling mutual inductance between the transmitters, since the transmitters are overlapped and located close to each other. M_{ij} is the mutual inductance between the ith transmitter and the jth transmitter ($M_{ij} = M_{ji}$).

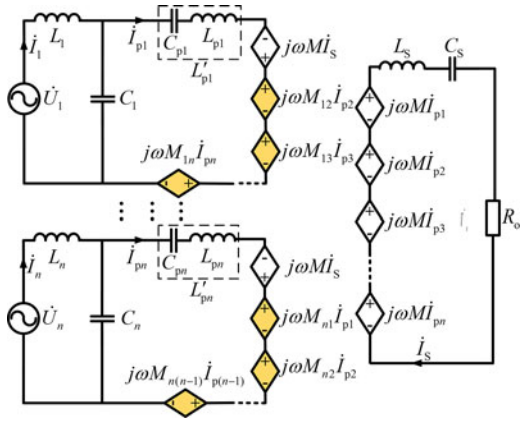

Fig. 7. Equivalent circuit of the proposed WPT system.

The equivalent circuit of the proposed WPT system is illustrated in Fig. 7. The magnetic coupling between transmitter #*i* and transmitter #*m* ($m = 1, 2 \ldots, i-1, i+1 \ldots n$) results in a non-negligible induced voltage within transmitter #*i*. The induced voltage can be expressed in phasor forms as follows:

$$\dot{U}_{im} = j\omega M_{im}\dot{I}_{pm}. \tag{5}$$

Therefore, the total induced voltages within the transmitter #*i* caused by the other transmitters are given by

$$\dot{U}_{Ti} = \sum_{m=1}^{i-1} j\omega M_{im}\dot{I}_{pm} + \sum_{m=i+1}^{n} j\omega M_{im}\dot{I}_{pm}. \tag{6}$$

It is clear that these induced voltages within each transmitter, because of the *LCL* resonant network, cause a large current with the corresponding inverter which increases the current stress of the semiconductor devices [38], [39]. It is significant to eliminate the total induced voltages caused by mutual couplings between the transmitters. One of the alternatives is to adopt an additional capacitor connected in series with the transmitter. When the voltage of the additional capacitor is a reverse voltage against the total induced voltages caused by the mutual coupling, the effect of the mutual coupling can be suppressed eventually.

To simplify, all the transmitter currents are assumed to be identical, i.e., $\dot{I}_{p1} = \cdots = \dot{I}_{pi} = \cdots \dot{I}_{pn}$. Then, the total induced voltages can be rewritten as

$$\dot{U}_{Ti} = j\omega\dot{I}_{pi}\left(\sum_{m=1}^{i-1} M_{im} + \sum_{m=i+1}^{n} M_{im}\right). \tag{7}$$

The voltage of the additional capacitor C_{ki} added in the ith transmitter can be derived as

$$\dot{U}_{ki} = \frac{\dot{I}_{pi}}{j\omega C_{ki}}. \tag{8}$$

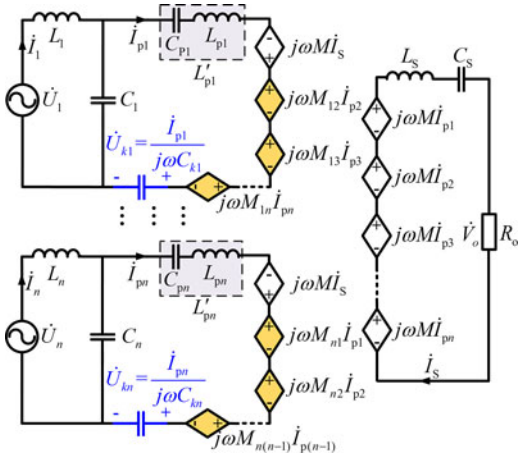

Fig. 8. Equivalent circuit with additional capacitors.

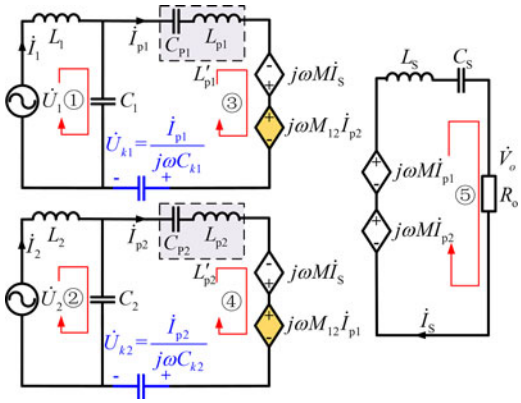

Fig. 9. Equivalent circuit of the WPT system based on two transmitters with additional capacitors.

In order to suppress the total induced voltage by the additional capacitor, the voltage of the additional capacitor should be with the same amplitude but a different polarity as shown in Fig. 8.

Therefore, the value of the additional capacitor can be expressed as

$$C_{ki} = \frac{1}{\omega^2 \left(\sum_{m=1}^{i-1} M_{im} + \sum_{m=i+1}^{n} M_{im} \right)}. \tag{9}$$

It should be noted that in the rest of this paper, the study case is focused on the WPT system composed of two transmitters for simplifying analysis. The analysis performed can be extended to multiple transmitters based WPT systems without loss of generality. Then, the equivalent circuit of the WPT system based on two transmitters can be depicted as Fig. 9.

III. Transmitter Currents Analysis

A. Modeling Analysis

According to Fig. 9, Kirchhoff's voltage law is applied to describe the relationship of voltages that are included in the loops ①–②. Therefore, we can get

$$\begin{bmatrix} 0 \\ 0 \\ 0 \\ 0 \\ 0 \end{bmatrix} = \begin{bmatrix} j\omega L_1 \dot{I}_1 + \dot{U}_{C1} - \dot{U}_1 \\ j\omega L_2 \dot{I}_2 + \dot{U}_{C2} - \dot{U}_2 \\ j\omega L'_{p1} \dot{I}_{p1} - j\omega M \dot{I}_s + j\omega M_{12} \dot{I}_{p2} + \dot{U}_{k1} - \dot{U}_{C1} \\ j\omega L'_{p2} \dot{I}_{p2} - j\omega M \dot{I}_s + j\omega M_{12} \dot{I}_{p1} + \dot{U}_{k2} - \dot{U}_{C2} \\ \dot{I}_s R_o - j\omega M \dot{I}_{p1} - j\omega M \dot{I}_{p2} \end{bmatrix}. \tag{10}$$

The inverter currents, the currents of the corresponding transmitters, and the current of the receiver can be derived as

$$\begin{bmatrix} \dot{I}_1 \\ \dot{I}_2 \\ \dot{I}_{p1} \\ \dot{I}_{p2} \\ \dot{I}_s \end{bmatrix} = \begin{bmatrix} \dfrac{\dot{U}_1 - \dot{U}_{C1}}{j\omega L_1} \\ \dfrac{\dot{U}_2 - \dot{U}_{C2}}{j\omega L_2} \\ \dfrac{\dot{U}_{C1} + j\omega M \dot{I}_s - j\omega M_{12} \dot{I}_{p2} - \dot{U}_{k1}}{j\omega L'_{p1}} \\ \dfrac{\dot{U}_{C2} + j\omega M \dot{I}_s - j\omega M_{12} \dot{I}_{p1} - \dot{U}_{k2}}{j\omega L'_{p2}} \\ \dfrac{j\omega M \dot{I}_{p1} + j\omega M \dot{I}_{p2}}{R_o} \end{bmatrix}. \tag{11}$$

According to (9), the additional capacitors can be calculated as

$$\begin{bmatrix} C_{k1} \\ C_{k2} \end{bmatrix} = \begin{bmatrix} \dfrac{1}{\omega^2 M_{12}} \\ \dfrac{1}{\omega^2 M_{12}} \end{bmatrix}. \tag{12}$$

Therefore, the voltages of the additional capacitors can be derived as

$$\begin{bmatrix} \dot{U}_{k1} \\ \dot{U}_{k2} \end{bmatrix} = \begin{bmatrix} \dfrac{\dot{I}_{p1}}{j\omega C_{k1}} \\ \dfrac{\dot{I}_{p2}}{j\omega C_{k2}} \end{bmatrix} = \begin{bmatrix} -j\omega M_{12} \dot{I}_{p1} \\ -j\omega M_{12} \dot{I}_{p2} \end{bmatrix}. \tag{13}$$

Substituting (13) into (11), the inverter currents, the currents of the corresponding transmitters, and the current of the receiver can be derived as

$$\begin{bmatrix} \dot{I}_1 \\ \dot{I}_2 \\ \dot{I}_{p1} \\ \dot{I}_{p2} \\ \dot{I}_s \end{bmatrix} = \begin{bmatrix} \dfrac{\dot{U}_1 - \dot{U}_{C1}}{j\omega L_1} \\ \dfrac{\dot{U}_2 - \dot{U}_{C2}}{j\omega L_2} \\ \dfrac{\dot{U}_{C1} + j\omega M \dot{I}_s - j\omega M_{12} \dot{I}_{p2} + j\omega M_{12} \dot{I}_{p1}}{j\omega L'_{p1}} \\ \dfrac{\dot{U}_{C2} + j\omega M \dot{I}_s - j\omega M_{12} \dot{I}_{p1} + j\omega M_{12} \dot{I}_{p2}}{j\omega L'_{p2}} \\ \dfrac{j\omega M \dot{I}_{p1} + j\omega M \dot{I}_{p2}}{R_o} \end{bmatrix}. \tag{14}$$

$$\begin{bmatrix}\dot{U}_{C1}\\ \dot{U}_{C2}\end{bmatrix}=\begin{bmatrix}\dfrac{\dot{I}_1-\dot{I}_{p1}}{j\omega C_1}\\ \dfrac{\dot{I}_2-\dot{I}_{p2}}{j\omega C_2}\end{bmatrix}. \tag{15}$$

The voltage induced in the receiver can be derived as

$$\dot{V}_o=j\omega M\dot{I}_{p1}+j\omega M\dot{I}_{p2}=j\omega M\left(\dot{I}_{p1}+\dot{I}_{p2}\right). \tag{16}$$

In a practical WPT system, it is difficult to let L_1 be equal to L_2 and have C_1 be equal to C_2 due to the inevitable component tolerances. For simplifying the analysis, assuming the tolerance of L_1 and L_2 is identical to α but with opposite bias and the tolerance of C_1 and C_2 is identical to α. Then, we can get

$$\begin{cases}C_1=(1+\alpha)C\\ C_2=(1-\alpha)C\\ L_1=(1+\alpha)L\\ L_2=(1-\alpha)L\\ \omega=\frac{1}{\sqrt{LC}}\end{cases}. \tag{17}$$

For convenience, the following variables are defined

$$\begin{aligned}A&=M^2\omega^2\left[\left(\alpha^4+4\right)\left(4M-L'_{p1}-L'_{p2}\right)+2L\left(\alpha^2-2\right)\right]\\ B&=R_o^2\omega^2\left\{L\left[\left(\alpha^2-2\right)\left(L'_{p1}+L'_{p2}-2M\right)\right.\right.\\ &\quad\left.\left.+\alpha^3\left(L'_{p1}-L'_{p2}\right)\right\}\right]\\ &\quad+\left(\alpha^4+4\right)\left(ML'_{p1}+ML'_{p2}-L'_{p1}L'_{p2}\right)\\ &\quad+\left(\alpha^2-1\right)L^2\\ D_1&=L'_{p2}\left(2\alpha-\alpha^2-2\right)+L(\alpha-1)\\ D_2&=L'_{p1}\left(-\alpha^2-2\alpha-2\right)-L(\alpha+1).\end{aligned} \tag{18}$$

Substituting (15)–(18) into (14), the transmitter currents can be derived as

$$\begin{aligned}\begin{bmatrix}\dot{I}_{p1}\\ \dot{I}_{p2}\end{bmatrix}&=\frac{1}{A^2+B^2}\\ &\times\begin{bmatrix}\left[\left(AMR_o+BM^2\omega\right)\left(\alpha^2-2\alpha+2\right)+AR_oD_1\right]\dot{U}_1\\ +\left(AMR_o-BM^2\omega\right)\left(\alpha^2+2\alpha+2\right)\dot{U}_2\\ \left[\left(AMR_o+BM^2\omega\right)\left(\alpha^2+2\alpha+2\right)+AR_oD_2\right]\dot{U}_2\\ +\left(AMR_o-BM^2\omega\right)\left(\alpha^2-2\alpha+2\right)\dot{U}_1\end{bmatrix}\\ &-\frac{j}{A^2+B^2}\\ &\times\begin{bmatrix}\left[\left(BMR_o+AM^2\omega\right)\left(\alpha^2-2\alpha+2\right)+BR_oD_1\right]\dot{U}_1\\ +\left(BMR_o-AM^2\omega\right)\left(\alpha^2+2\alpha+2\right)\dot{U}_2\\ \left[\left(BMR_o+AM^2\omega\right)\left(\alpha^2+2\alpha+2\right)+BR_oD_2\right]\dot{U}_2\\ +\left(BMR_o-AM^2\omega\right)\left(\alpha^2-2\alpha+2\right)\dot{U}_1\end{bmatrix}.\end{aligned} \tag{19}$$

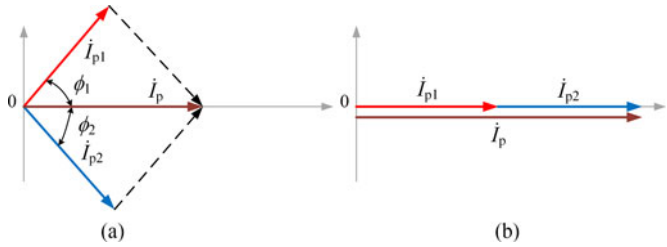

Fig. 10. Current phasor diagram.

The current difference between the transmitters can be expressed as

$$\begin{aligned}\dot{I}_c&=\dot{I}_{p1}-\dot{I}_{p2}\\ &=\frac{1}{A^2+B^2}\left\{\begin{matrix}\left[2BM^2\omega\left(\alpha^2-2\alpha+2\right)+AR_oD_1\right]\dot{U}_1\\ -\left[2BM^2\omega\left(\alpha^2+2\alpha+2\right)+AR_oD_2\right]\dot{U}_2\end{matrix}\right\}\\ &-\frac{j}{A^2+B^2}\left\{\begin{matrix}\left[2AM^2\omega\left(\alpha^2-2\alpha+2\right)+BR_oD_1\right]\dot{U}_1\\ -\left[2AM^2\omega\left(\alpha^2+2\alpha+2\right)+BR_oD_2\right]\dot{U}_2\end{matrix}\right\}.\end{aligned} \tag{20}$$

It is evident that the transmitter currents are not identical in phasor forms with the phase difference and the magnitude difference due to the component tolerance, gate driver delay, and other uncertainties. Some slight differences present in the output voltages of the inverters, which will result in a large transmitter current difference damaging the semiconductor, introducing conduction losses in the circuit, and detuning the whole system, will be investigated in the following section.

B. *Effects of the Transmitter Currents Differences*

As depicted in Fig. 10(a), the phase angles of the transmitter currents are not equal to zero. Under this condition, the total current $\dot{I}_p=\dot{I}_{p1}+\dot{I}_{p2}$ which is less than the condition shown in Fig. 10(b) with the same magnitude of two transmitter currents as $\phi_1=\phi_2=0$. According to (16), the difference in the phase of the transmitter currents results in a lower induced voltage in the receiver. Especially, when there is 180 degree phase difference between two transmitter currents with the same magnitude, no magnetic field exists. As a result, no power can be transferred if the transmitter currents are completely out of phase, due to being completely suppressed at the receiver. In order to increase the induced voltage in the receiver, larger transmitter currents with different phases are needed to generate the same magnetic field compared to that with in phase currents. It will bring extra power losses in the transmitters and the corresponding inverter, consequently, decreasing the power efficiency.

Therefore, in order to improve the performance of the proposed WPT system, the transmitter currents should be controlled in phase, i.e., $\phi_1=\phi_2=0$.

Additionally, the induced voltages within each transmitters generated by the mutual cross couplings can only be efficiently suppressed by the additional capacitors with the assumption that all the transmitters' currents are the same. Therefore, not only the phases but also the amplitudes of the transmitter currents should be controlled to be identical. In order to improve the

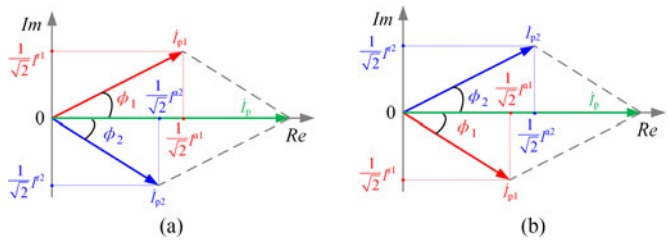

Fig. 11. Diagram of current decomposition (a) $\dot{I}_{p2}$ lags behind $\dot{I}_{p1}$, and $\dot{I}_{p1}$ lags behind $\dot{I}_{p2}$.

transmitted power and eliminate the effects of the mutual cross couplings, it is desirable to investigate an effective and practical approach to control all the transmitter currents to be identical.

IV. Transmitter Current Decomposition Based Control Method for the Proposed WPT System

As discussed above, it is significant to control the amplitudes and phases of the transmitter currents. Unfortunately, the phase detection circuits are not applicable under a small-current condition. Meanwhile, it is not easy to tune the resonant circuit at the resonant frequency in practical WPT systems, which results in the transmitter current being distorted. Therefore, the zero crossing point is not the zero phase of the fundamental current and it will result in a misunderstanding of the phase of the transmitter current.

Fortunately, the current signal can be represented as a phasor form which consists of active current component and reactive current component as shown in Fig. 11. Alternatively, the decomposed active and reactive currents can be represented by a linear function instead of detecting the current amplitude and phase angle.

i_p can be fixed to the real axis as the reference signal according to the SM, and the transmitter currents can be decomposed into active and reactive components against the reference signal i_p as shown in Fig. 11. An orthogonal current constructed by using i_p with $\pi/2$ phase shift is adopt to calculate the decomposed components. To improve the reliability of the control system, i_p is chosen as the reference signal. The reference signal is not easy to be absent, when a fault occurs in an inverter unit.

A. Decomposition of Current Into Virtual Active and Reactive Current Components

The sum of the transmitter currents i_p is feasible to be assumed as a pure sinusoidal signal due to the resonant network, which can be set as the reference signal with a zero phase:

$$i_p = I_m \sin(\omega t) \tag{21}$$

where I_m is the amplitude of the current i_p.

The phasor form of i_p without imaginary component can be expressed as

$$\dot{I}_p = \frac{1}{\sqrt{2}} I_m. \tag{22}$$

The current of the kth $(k = 1, 2)$ transmitter with the phase of ϕ_k can be defined as

$$\begin{aligned} i_{pk} &= I_{mk} \sin(\omega t + \phi_k) \\ &= I_{mk} \cos(\phi_k) \sin(\omega t) + I_{mk} \sin(\phi_k) \cos(\omega t) \end{aligned} \tag{23}$$

where I_{mk} is the amplitude of the current i_{pk}, and ϕ_k is the initial phase of the current i_{pk} against i_p. $I_{mk}\cos(\phi_k)\sin(\omega t)$ and $I_{mk}\sin(\phi_k)\cos(\omega t)$ are defined as the active and reactive current components.

The phasor form of the kth $(k = 1, 2)$ transmitter current can be expressed as

$$\dot{I}_{pk} = \frac{1}{\sqrt{2}} I^{ak} + j \frac{1}{\sqrt{2}} I^{rk}. \tag{24}$$

In addition, I^{ak} and I^{rk} are the amplitude of the active and reactive current components as per i_p as shown in Fig. 11, which can be expressed as

$$\begin{bmatrix} I^{ak} \\ I^{rk} \end{bmatrix} = \begin{bmatrix} I_{mk} \cos(\phi_k) \\ I_{mk} \sin(\phi_k) \end{bmatrix}. \tag{25}$$

Therefore, I^{ak} and I^{rk} can represent the amplitude and phase angle of the transmitter current i_{pk}. The reference current $\dot{I}_p$ is constructed of the transmitter current phasors $\dot{I}_{p1}$ and $\dot{I}_{p2}$ through the parallelogram law. It can be figured out that I^{a1} and I^{a2} must be both positive. I^{r1} and I^{r2} must be of different polarities as shown Fig. 11.

By delaying the phase of the total current i_p by $\pi/2$, we can get another reference current as

$$i_p^t = I_m \sin\left(\omega t + \frac{\pi}{2}\right) = I_m \cos(\omega t). \tag{26}$$

Virtual active and reactive powers of the kth transmitter current i_{pk} against the total current i_p are defined here. It should be emphasized here that the virtual active and reactive powers are not the circuit and/or physical reactions in the real system, and it is just a mathematic method for calculating the active and reactive current components against i_p. The defined virtual active and reactive powers are expressed as

$$\begin{bmatrix} P_k \\ Q_k \end{bmatrix} = \begin{bmatrix} \mathrm{Re}\left[\dot{I}_p \cdot \left(\dot{I}_{pk}\right)^*\right] \\ \mathrm{Im}\left[\dot{I}_p \cdot \left(\dot{I}_{pk}\right)^*\right] \end{bmatrix} = \begin{bmatrix} \dfrac{I_m I^{ak}}{2} \\ -\dfrac{I_m I^{rk}}{2} \end{bmatrix} \tag{27}$$

where $(\mathbf{A})^*$ represents the conjugate operation of $\mathbf{A}$.

The multiplication of (21) and (26) by the kth transmitter current i_{pk} and the current i_p, respectively, can be derived as

$$\begin{aligned} \begin{bmatrix} i_{pk}^s \\ i_{pk}^c \end{bmatrix} &= \begin{bmatrix} i_{pk} & 0 \\ 0 & i_{pk} \end{bmatrix} \begin{bmatrix} i_p & 0 \\ 0 & i_p^t \end{bmatrix} \\ &= \begin{bmatrix} \dfrac{-I_{mk} I_m [\cos(2\omega t + \phi_k) - \cos(\phi_k)}{2} \\ \dfrac{I_{mk} I_m [\sin(2\omega t + \phi_k) - \sin(\phi_k)}{2} \end{bmatrix} \end{aligned} \tag{28}$$

$$i_p^s = i_p \cdot i_p = \frac{-{I_m}^2 [\cos(2\omega t) - 1]}{2}. \tag{29}$$

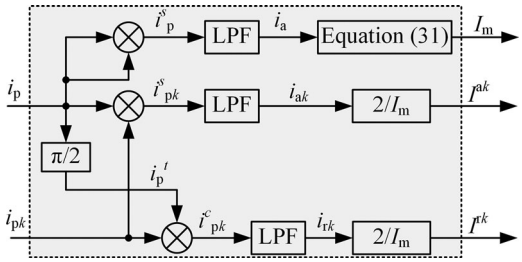

Fig. 12. Block diagram of the proposed CDM.

It is evident that i^s_{pk}, i^c_{pk}, and i^s_p are composed of dc component and a second-order harmonic component. By adopting an appropriate low-pass filter (LPF), the second-order harmonic component can be efficiently filtered out. In the paper, a second-order Butterworth filter with the cut off frequency of 100 Hz has been used as the LPF. Therefore, the dc component can be obtained as shown in the following equation:

$$\begin{bmatrix} i_{ak} \\ i_{rk} \\ i_a \end{bmatrix} = \begin{bmatrix} \dfrac{I_{mk} I_m \cos(\phi k)}{2} \\ \dfrac{I_{mk} I_m \sin(\phi k)}{2} \\ \dfrac{I_m^2}{2} \end{bmatrix}. \tag{30}$$

As a result, the amplitude of i_p can be expressed as

$$I_m = \sqrt{2 i_a}. \tag{31}$$

Substituting (25) and (30) into (27), the virtual active and reactive powers can be rewritten as

$$\begin{bmatrix} P_k \\ Q_k \end{bmatrix} = \begin{bmatrix} i_{ak} \\ i_{rk} \end{bmatrix} = \begin{bmatrix} \dfrac{I_{mk} I_m \cos(\phi_k)}{2} \\ \dfrac{I_{mk} I_m \sin(\phi_k)}{2} \end{bmatrix}. \tag{32}$$

Substituting (31) and (32) into (27), the amplitudes of the active and reactive current components can be derived as

$$\begin{bmatrix} I^{ak} \\ I^{rk} \end{bmatrix} = \begin{bmatrix} \dfrac{\sqrt{2} i_{ak}}{\sqrt{i_a}} \\ \dfrac{\sqrt{2} i_{rk}}{\sqrt{i^s{}_a}} \end{bmatrix}. \tag{33}$$

Therefore, the amplitudes of the active and reactive current components of the corresponding transmitter current against the reference signal can be calculated by the proposed decomposition method named current decomposition method (CDM), which is shown in Fig. 12.

B. Transmitter Current Control Diagram

The transmitter current control strategy for two-transmitter WPT system based on the CDM is shown in Fig. 13. As depicted in Figs. 8 and 9, in order to control the transmitter currents in phase with each other, the amplitude of reactive currents should be controlled to be zero. The transmitter current differences can be mitigated by sophisticatedly controlling the amplitude and angle of each inverter's output voltage indirectly [40]. This control strategy is composed of two control feedback loops for each inverter, the active and reactive currents control loops. A proportional-integral controller (reactive current controller) is adopted for the reactive current control loop by setting the amplitude of references reactive current $I^{rk} = 0$. At the steady state, all the transmitter currents are controlled in phase, which indicates $I^{rk} = 0$. Assuming that a perturbation occurs in the phase of the transmitter currents and taking two transmitters based WPT system, e.g., $I^{r1} > 0$ and $I^{r2} < 0$, the outputs of the reactive current controller θ_1 decrease and θ_2 increase. However, if the absolute magnitude of I^{r1} and I^{r2} is used in the reactive current controller ($|I^{r1}| > 0$ and $|I^{r2}| > 0$), the reactive current control loop will be out of order because the polarity of the reactive currents is absent. As a result, the transmitter currents can be controlled in phase efficiently by controlling the phases of the inverters output voltages indirectly.

In practical WPT applications, the output voltage of the receiver should be regulated at a constant value for various applications. Therefore, the active current control loop is composed of two controllers which are the internal active current sharing controller and the outer output voltage controller. The amplitude of active current reference is the sum of the active current reference $\sum_{j=1}^{2} I^{aj} / \sum_{j=1}^{2} a_j$ and output of the outer output voltage controller and the output voltage reference is u_o^*, where a_j is the fault signal of the jth inverter unit. In order to improve the proposed WPT system's reliability, each inverter is equipped with a dedicated fault detection module, which will send signal $a_j = 0$ to the jth protection device in order to disconnect the jth fault unit from the whole system when a fault occurs in the jth inverter unit. If the inverter unit is normally operating, $a_j = 1$ is sent. For example, if a fault occurs in the inverter unit #2, then both I^{a2} and a_2 will be zero ($I^{a2} = 0$, $a_2 = 0$). However, I^{a1} and a_1 will not be zero ($I^{a1} \neq 0$, $a_1 = 1$) because the inverter unit #1 is normally operating. Then, the amplitude of active current references will be $(I^{a1} + I^{a2})/(a_1 + a_2) = (I^{a1} + 0)/(1 + 0) = I^{a1}$. Similarly, when no fault occurs, the amplitude of active current reference is $I^{ak*} = \frac{1}{2}\sum_{j=1}^{2} I^{aj}$. Meanwhile, the amplitude of reactive current reference is still zero and the reference of the output voltage is not changed, which can maintain the whole system working continually. Thus, the reliability and availability of the IPT system can be dramatically improved. A wireless signal communication module (NRF24L01 +) is adopt to send the measured output voltage (u_o) of the receiver for the closed-loop control [41].

Assuming that a perturbation occurs in the amplitude of the transmitter currents, e.g., I^{a1} increases and I^{a2} decreases ($I^{a1} > I^{a2}$), the output of internal active current sharing controller #1 decreases and the output of internal active current sharing controller #2 increases. Finally, the outputs of the active current loop δ_1 decrease and δ_2 increase. Consequently, the amplitude of the inverter #1 output voltage decreases, and the amplitude of the inverter #2 output voltage increases.

Owing to the active and reactive currents control loops, the transmitter currents can be controlled to be identical and the output voltage can be regulated in the secondary side. The control strategy can also be extended to multiple transmitters based WPT systems easily.

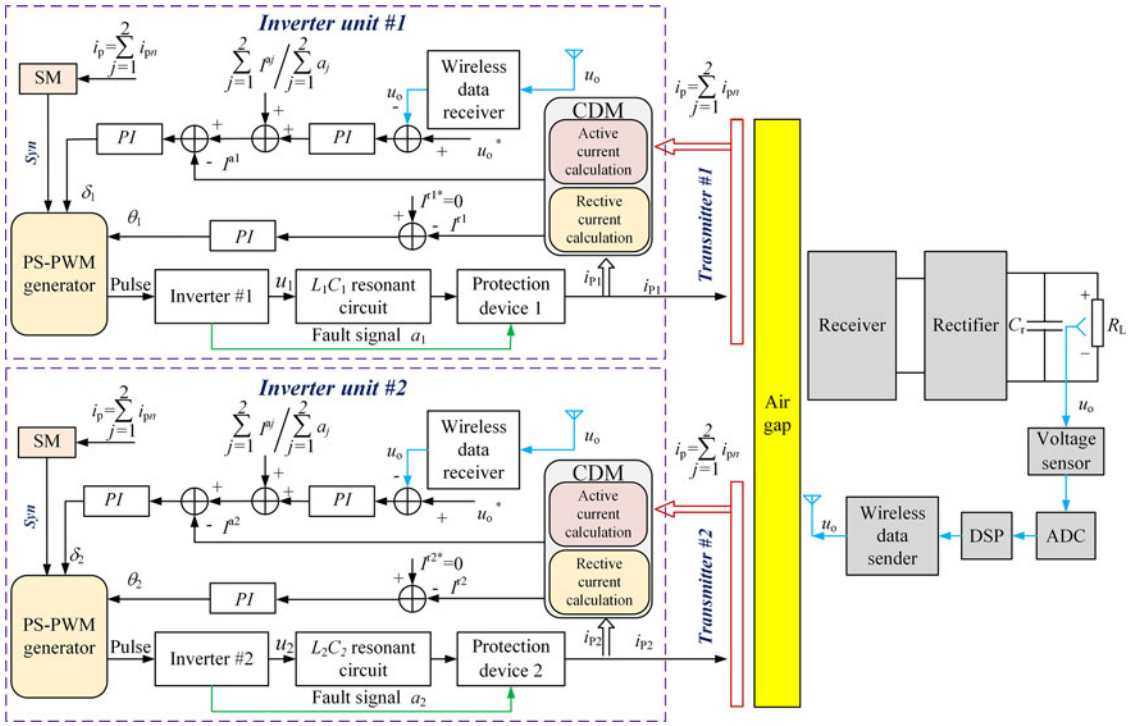

Fig. 13. Control diagram for the two-transmitter WPT system.

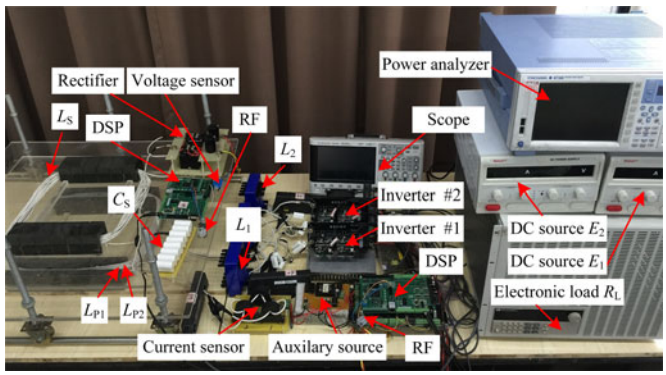

Fig. 14. Exterior appearance of the proposed WPT prototype.

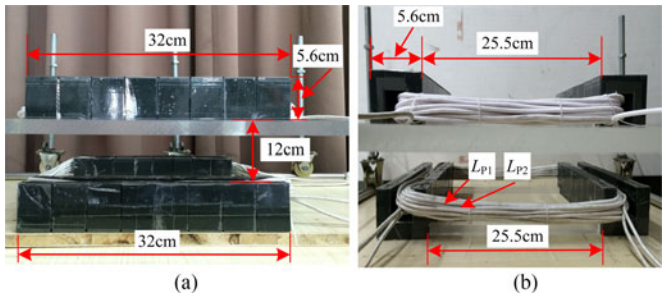

Fig. 15. Transmitters and the receiver wound with Litz wire. (a) Lateral view, and (b) front view of the coils.

V. Experimental Results

A. Prototype System

In order to verify the performance of the proposed control method for the WPT system based on multiple transmitters, an experimental prototype WPT system, comprising two transmitters, two resonant inverters, and a single receiver, was built in the laboratory settings as shown in Fig. 14. The proposed controller in Fig. 13 was implemented in a TMS320F28335 digital signal processing unit. CONCEPT-2SC0108T2A0-17 was adopted as the power MOSFET driver to fulfill the requirement of high switching frequency in the experiment. Moreover, it has a function of fault detection. The transmitters and the receiver were wound around ferrite cores with Litz wires. The coupler was built with $N_1 = 10$ turns for the dual transmitters and $N_2 = 20$ turns for the receiver. It is worth noticing that the ferrite cores can be any other types, and in this paper they were U-type ferrite cores as shown in Fig. 15. The air gap between the transmitters and the receiver was set to be 12 cm. The mutual and self-inductance of the transmitters and receiver were measured by Agilent E4980A *LCR* meter. An electronic load was applied as the load connected to the receiver.

The circuit parameters of the experimental setup are listed in Table I. In addition, in the experimental evaluation, it is assumed that the inverters have the same power rating and the transmitters have the same structure.

B. Experimental Results

1) Misalignment Analysis: The measured mutual inductances between the transmitters and the receiver at different lateral offsets are shown in Fig. 16. These lateral offset variations only cause the variations of the mutual inductance between the transmitters and the receiver. If the lateral offset is increased

TABLE I
DESIGN SPECIFICATIONS AND CIRCUIT PARAMETERS OF WPT PROTOTYPE

Parameters	Value
Inverter frequency f/kHz	20
DC voltage of the invert unit E_1 and E_2/V	120
The transmitter inductance of inverter #1 L_{p1}/μH	165.4
The transmitter inductance of inverter #2 L_{p2}/μH	163.5
The resonant capacitance of inverter #1 C_1/nF	550.6
The resonant inductance of inverter #2 C_2/μH	450.5
The resonant inductance of inverter #1 L_2/μH	138
The resonant inductance of inverter #2 L_2/μH	117
Compensation capacitance of inverter #1 C_{p1}/nF	246.1
Compensation capacitance of inverter #2 C_{p2}/nF	268.2
Mutual inductance of the transmitter #1 and receiver M_{1s}/μH	63.1
Mutual inductance of the transmitter #2 and receiver M_{2s}/μH	62.4
Mutual inductance of the transmitter #1 and transmitter #2 M_{12}/μH	159.7
The additional capacitor in transmitter #1 C_{k1}/nF	396.5
The additional capacitor in transmitter #2 C_{k2}/nF	396.5
Inductance of the receiver L_s/μH	506.2
Resonant compensation capacitance of receiver C_s/nF	124.8
MOSFET: IRFN 640N	

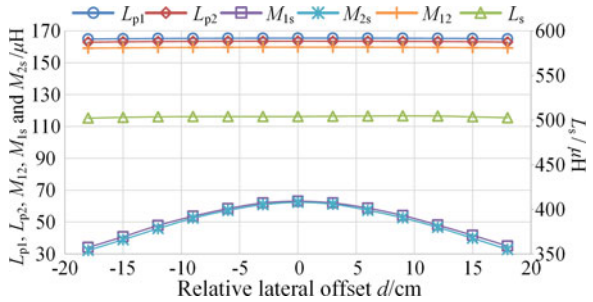

Fig. 16. Mutual inductances and self-inductances versus lateral offset between the transmitters and receiver.

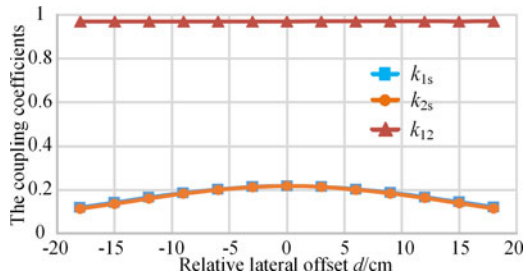

Fig. 17. Coupling coefficients versus lateral offset between the transmitters and receiver.

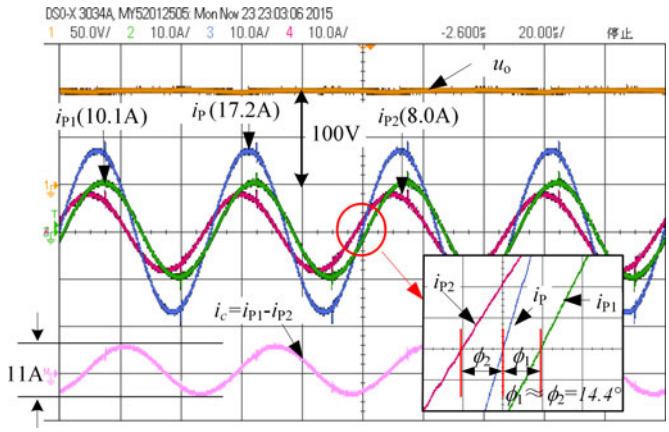

Fig. 18. Current waveforms and the output voltage waveform without transmitter current control.

from 0 to 20 cm, the mutual inductances (M_{1S} and M_{2S}) are reduced from 63.1 μH (62.4 μH) to34.8 μH (33.8 μH). Owing to the identical structure of the transmitters, the variations of the mutual inductance M_{1S} and M_{2S} with the lateral offset are approximately identical. The measured self-inductances L_{p1} and L_{p2} are depicted in Fig. 16. L_{p1} and L_{p2} vary by a slight difference as small as 0.03% compared to its peak value of 165.4 μH, and L_s keeps stable at 506 μH. The mutual inductance between the transmitters (M_{12}) keeps stable at 159.7 μH with different lateral offsets. The coupling coefficients $k_{1s} = \frac{M_{1s}}{\sqrt{L_{p1}L_s}}, k_{2s} = \frac{M_{2s}}{\sqrt{L_{p2}L_s}}$, $k_{12} = \frac{M_{12}}{\sqrt{L_{p1}L_{p2}}}$ are depicted in Fig. 17. As a result, the additional capacitors can mitigate the effects of the mutual cross coupling between the transmitters with different lateral offsets.

2) Inverter Units With Asymmetrical Resonant Components: In a practical WPT system based on multiple transmitters, it is unlikely that all the parameters of each resonant inverter are identical. Especially, the tolerance for high-quality commercial inductors and capacitors is about 20%. It is assumed that the experimental setup has a 20% difference in the inductors (L_1 and L_2) and an approximate 20% difference in the capacitors (C_1 and C_2).

Case I (alignment and without transmitter current control): Fig. 18 shows the steady-state experiment waveforms without current phase control [the same δ and θ as shown in (3)]. The output voltage of the receiver is controlled to be 100 V by only controlling the magnitude of the inverters output voltage, and the load connected to the receiver is 7 Ω. As can be seen from Fig. 18, both the phases and the amplitudes of the transmitter currents are different, and the amplitude of the difference ($i_{p1} - i_{p2}$) of the transmitter currents is about 5.5 A shown in the bottom of Fig. 18. The phase difference of the transmitter currents is about 28.8°. Therefore, the current difference brings an extra power loss of the WPT system and results in an unevenly power distribution between the transmitters. In addition, the additional capacitors added in the transmitters cannot efficiently mitigate the effect of the mutual cross coupling between the transmitters due to the transmitter current difference.

The input power of each inverter and the load power are measured by a power analyzer (YOKOGAWA-WT1800) as shown in Fig. 19. It is clear that there is about 210 W power difference between the two inverters with the same input dc voltage due to the current difference caused by the tolerance of the circuit parameters. The overall efficiency from dc power supply to the electronic load is 88.78% measured by the power analyzer.

Case II (alignment and with transmitter current control): In order to eliminate the current difference and increase the overall efficiency of the proposed WPT system, the proposed transmitter current control method is applied to the experimental setup. The experimental waveforms can be seen in Fig. 20. The

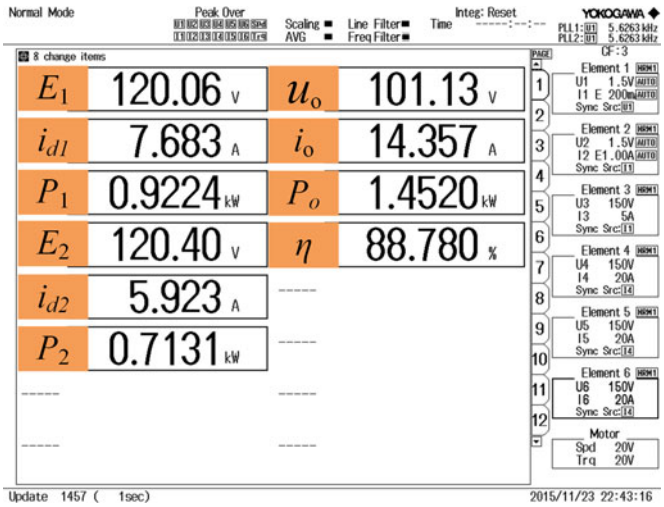

Fig. 19. Capture of power from power analyzer without transmitter current control.

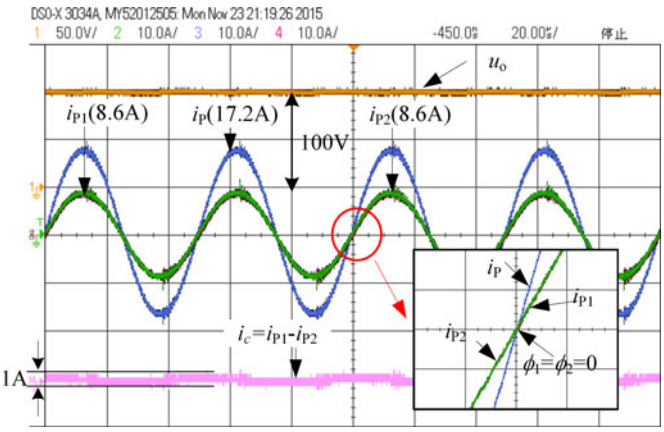

Fig. 20. Current waveforms and the output voltage waveform with transmitter current control.

Fig. 21. Capture of power from power analyzer with transmitter current control.

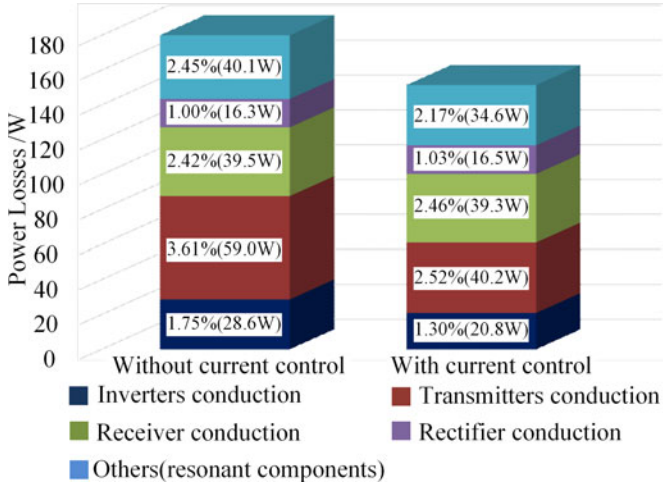

Fig. 22. Measured power loss distribution at 1.44 kW output with transmitter current control.

output voltage of the receiver is regulated to be 100 V and the load is also 7 Ω as shown previously. The currents of the transmitters are totally identical and the current difference can be efficiently minimized to be approximate 0.5 A. The induced voltages caused by the mutual crossing coupling between the transmitters can be mitigated by the additional capacitors. As shown in Fig. 21, the input powers of the two inverters (801.5 W for invert unit #1 and 799.5 W for inverter unit #2) are almost identical with just 1 W difference, due to the slight difference (0.7 μH) between M_{1s} and M_{2s}. It is evident that the transmitted power can be enhanced up to 1.45 kW by using two resonant inverters with a power rating of 850 W. Meanwhile, the overall power loss is about 155 W, and the measured power loss distribution is shown in Fig. 22 for both cases. For case I, the current difference between the transmitters is larger, and hence, the conduction losses on inverters, transmitters, and resonant components are higher. Furthermore, the overall efficiency of the case II is up to 90.34%, which is 1.52% higher than that without the proposed transmitter current control. As expected, the overall efficiencies of the proposed WPT system with transmitter current control are higher than those without transmitter current control shown in Fig. 23 under various output power conditions.

The performances of the proposed WPT system with transmitter current control against various lateral offset between the transmitters and receiver can be seen in Fig. 24. The power sharing can be achieved with transmitter current control against different lateral offsets. The efficiency declines with the increase of the lateral offset as the mutual inductances (M_{1S} and M_{2S}) drop.

3) Dynamic Performances of the Proposed Transmitter Current Control Method: It is important and necessary to investigate the dynamic performances of the proposed control method. Fig. 25 shows the output voltage waveform, the currents waveforms of the two transmitters, and the amplitude of reactive current of i_{p1} (calculated by the controller and displayed by the digital to analog converter). As shown in Fig. 25, the output voltage decreases from 100 to 80 V with a fast transient of

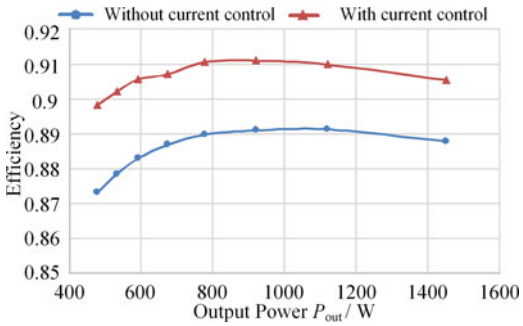

Fig. 23. Measured overall efficiencies with/without transmitter current control.

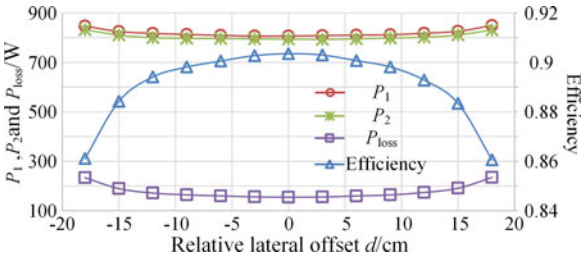

Fig. 24. Efficiency and power losses with transmitter current control versus lateral offset between the transmitters and receiver.

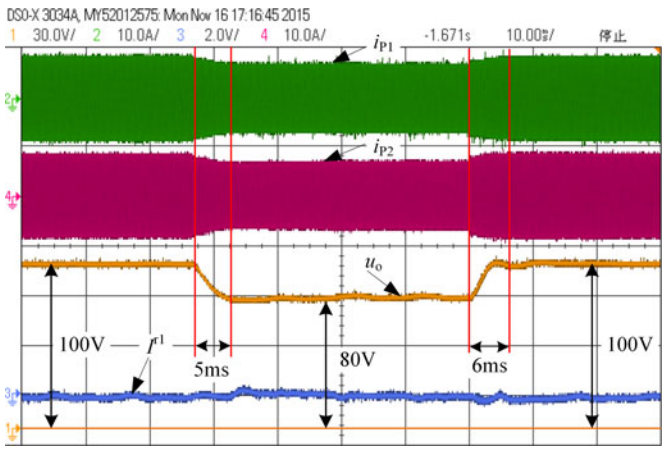

Fig. 25. Dynamic tracking process of the transmitter current control strategy.

5 ms following the changes in the reference signal, and raises from 80 V back to 100 V with a very fast response time of 6 ms without overshoot. Therefore, the output voltage can be tightly controlled by the proposed control method. Moreover, the amplitudes of the transmitter currents are regulated to be identical not only in steady-states but also in transient states, and the amplitude of reactive current of i_{p1} is controlled to be zero indicating the transmitter currents are completely controlled to be in phase.

The output voltage can be maintained to be a steady state of 100 V by changing the load resistance from 15 to 10 Ω and changing back to 15 Ω as shown in Fig. 26. The output voltage takes less than 7 ms to settle down in both cases, which indicates that a good dynamic performance can be achieved by the

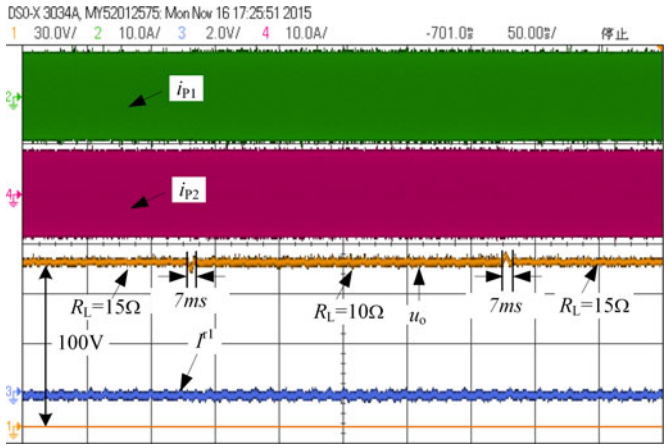

Fig. 26. Transient process of the transmitter current control strategy with load variations.

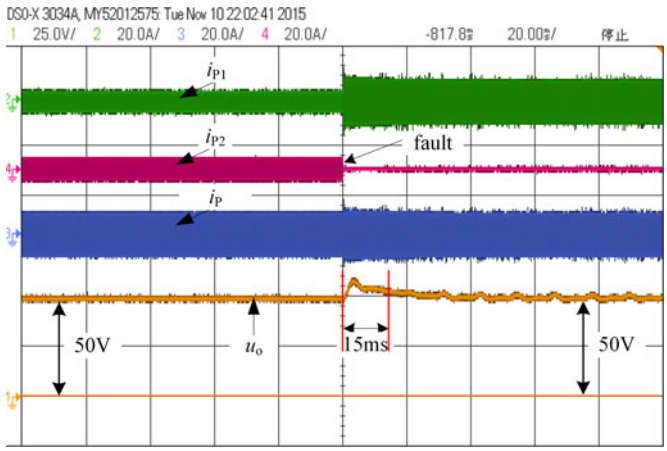

Fig. 27. Transient waveforms of the experimental system when a fault occurs in inverter #2.

proposed control method. It should be noted that the transmitter currents are controlled to be identical since the amplitudes and phases of the transmitter currents are identical under load variations cases.

4) Reliability Analysis: In order to evaluate the reliability of the proposed WPT system, it is desirable to investigate the performance of the system with faults. The transient waveforms of the experimental setup when a fault occurs in inverter unit #2 are shown in Fig. 27. The output voltage is supposed to be regulated to 50 V during normal operation. With the occurrence of fault in one of the inverters, the faulty inverter is discontented from the system by the protection device, and the output voltage can be maintained to be 50 V with a fast response time of 15 ms and with a slight transient overshoot by increasing the output power of inverter unit #1. Although the transmitter current i_{p2} decreases to zero, the load cannot feel any change from the power source and the system keeps working continuously, which proves the availability and reliability of the proposed method.

It should be noted that the power of the inverter unit #1 should increase to compensate the power loss of the disconnected inverter unit #2 in order to maintain the output voltage to be a

constant value. Under this condition, the components of the remaining systems need to be rated for the full load condition. In order to cut the cost of the whole system, the load of the WPT system should be operated in a degraded mode. For instance, the train should be slowed down under the faulty condition for degrading the power demand and the whole system can still work. It is clear that the multiple transmitters based WPT system is more reliable than traditional one.

C. Discussions and Future Plans

It should be emphasized that for low power applications such as wireless EV charging applications (3.3, 7.7, 22 kW, etc.), it is easy and economical to realize a WPT system with the traditional structure other than the proposed structure. Actually, the proposed method is indeed complex and impractical for low power applications where the traditional WPT system with single inverter and single transmitter can handle the required power. However, the demand for high-power WPT systems is on the rise, e.g., high-speed trains and rapidly charging system for public buses, implementation of such WPT systems using low-cost and low-power semiconductor devices has been a challenge. Our research goal is to use multiple relative "lower" power inverters to achieve a high power output for some high applications and improve the reliability of the WPT system.

A scale-down experimental setup assembled in the university's lab is provided to verify the proposed approach. The scaled-down power level is based on the capability and space limitation of our laboratory. This paper only theoretically and experimentally proves the 1.45 kW output power effectiveness by using two resonant inverters with a power rating of 850 W composed of low capacity semiconductors. Therefore, the maximum load voltage is only 100 V. Our future work is to install the designed WPT system on a real railway vehicle. In order to achieve that, we will not only adopt high power inverters to upgrade the total required power level, but also test the proposed control method when the vehicle is in motion. Then, the load voltages can be enhanced to meet the requirement of the real application.

VI. Conclusion

Multiple overlapped transmitters based WPT systems, which can upgrade the power capacity and improve the reliability of the WPT system for high power applications, have been described. Additional capacitors adopted in the transmitters are employed to suppress the effects of the mutual cross couplings among the transmitters. The current difference among transmitters in the proposed WPT system has been analyzed and described in detail. A transmitter current control method based on the CDM is presented to minimize the current difference and regulate the output voltage of the receiver. The availability and reliability of the proposed WPT system can be dramatically improved by the proposed control strategy.

A 1.5 kW experimental prototype is set up and tested. The experimental results verify the performance of the proposed control approach. The transmitted power of the proposed WPT system has been enhanced up to 1.45 kW by using two resonant inverters with a power rating of 850 W, and the overall efficiency of the proposed system is 90.34% which is 1.52% higher than that without the proposed transmitter current control. The output voltage can be regulated within 7 ms and the system keeps working continuously even with a fault.

References

[1] J. T. Boys, G. A. Covic, and A. W. Green, "Stability and control of inductively coupled power transfer systems," *IEE Proc. Electr. Power Appl.*, vol. 147, no. 1, pp. 37–43, Jan. 2000.

[2] D. J. Graham, J. A. Neasham, and B. S. Sharif, "Investigation of methods for data communication and power delivery through metals," *IEEE Trans. Ind. Electron.*, vol. 58, no. 10, pp. 4972–4980, Oct. 2011.

[3] Y. Li, R. Mai, M. Yang, and Z. He, "Cascaded multi-level inverter based IPT systems for high power applications," *J. Power Electron.*, vol. 15, no. 6, pp. 1508–1516, Nov. 2015.

[4] Y. Li, R. Mai, L. Lu, and Z. He, "A novel IPT system based on dual coupled primary tracks for high power applications," *J. Power Electron.*, vol. 16, no. 1, pp. 111–120, Jan. 2016.

[5] M. R. Amini and H. Farzanehfard, "Three-phase soft-switching inverter with minimum components," *IEEE Trans. Ind. Electron.*, vol. 58, no. 6, pp. 2258–2264, Jun. 2011.

[6] Y. L. Li, Y. Sun, and X. Dai, "μ-Synthesis for frequency uncertainty of the ICPT system," *IEEE Trans. Ind. Electron.*, vol. 60, no. 1, pp. 291–300, Jan. 2013.

[7] J. G. Bum and B. H. Cho, "An energy transmission system for an artificial heart using leakage inductance compensation of transcutaneous transformer," *IEEE Trans. Power Electron.*, vol. 13, no. 6, pp. 1013–1022, Nov. 1998.

[8] S. Ping, A. P. Hu, S. Malpas, and D. Budgettt, "A frequency control method for regulating wireless power to implantable devices," *IEEE Trans. Biomed. Circuits Syst.*, vol. 2, no. 1, pp. 22–29, Mar. 2008.

[9] K. W. Klontz, D. M. Divan, D. W. Novotny, and R. D. Lorenz, "Contactless power delivery system for mining applications," *IEEE Trans. Ind. Appl.*, vol. 31, no. 1, pp. 27–35, Jan./Feb. 1995.

[10] J. Kuipers, H. Bruning, S. Bakker, and H. Rijnaarts, "Near field resonant inductive coupling to power electronic devices dispersed in water," *Sens. Actuators A: Phys.*, vol. 178, pp. 217–222, May 2012.

[11] S. Hasanzadeh, S. Vaez-Zadeh, and A. H. Isfahani, "Optimization of a contactless power transfer system for electric vehicles," *IEEE Trans. Veh. Technol.*, vol. 61, no. 8, pp. 3566–3573, Oct. 2012.

[12] K. D. Papastergiou and D. E. Macpherson, "An airborne radar power supply with contactless transfer of energy-Part-II: Converter design," *IEEE Trans. Ind. Electron.*, vol. 54, no. 5, pp. 2885–2893, Oct. 2007.

[13] W. X. Zhong, C. Zhang, X. Liu, and S. Y. R. Hui, "A methodology for making a three-coil wireless power transfer system more energy efficient than a two-coil counterpart for extended transfer distance," *IEEE Trans. Power Electron.*, vol. 30, no. 2, pp. 933–942, Feb. 2015.

[14] J. P. C. Smeets, T. T. Overboom, J. W. Jansen, and E. A. Lomonova, "Comparison of position-independent contactless energy transfer systems," *IEEE Trans. Power Electron.*, vol. 28, no. 4, pp. 2059–2067, Apr. 2013.

[15] S. Lee, B. Choi, and C. T. Rim, "Dynamics characterization of the inductive power transfer system for online electric vehicles by Laplace phasor transform," *IEEE Trans. Power Electron.*, vol. 28, no. 12, pp. 5902–5909, Dec. 2013.

[16] W. Zhang, S. C. Wong, C. K. Tse, and Q. Chen, "Analysis and comparison of secondary series- and parallel-compensated inductive power transfer systems operating for optimal efficiency and load-independent voltage-transfer ratio," *IEEE Trans. Power Electron.*, vol. 29, no. 6, pp. 2979–2990, Jun. 2014.

[17] G. A. J. Elliot, S. Raabe, G. A. Covic, and J. T. Boys, "Multiphase pick-ups for large lateral tolerance contactless power-transfer systems," *IEEE Trans. Ind. Electron.*, vol. 57, no. 5, pp. 1590–1598, May 2010.

[18] J. Huh, S. W. Lee, W. Y. Lee, G. H. Cho, and C. T. Rim, "Narrow-width inductive power transfer system for online electrical vehicles," *IEEE Trans. Power Electron.*, vol. 26, no. 12, pp. 3666–3679, Dec. 2011.

[19] S. Boyune *et al.*, "Design of a high power transfer pickup for on-line electric vehicle (OLEV)," in *Proc. IEEE Int. Electr. Veh. Conf.*, 2012, pp. 1–4

[20] S. Chopra and P. Bauer, "Driving range extension of EV with on-road contactless power transfer—A case study," *IEEE Trans. Ind. Electron.*, vol. 60, no. 1, pp. 329–338, Jan. 2013.
[21] J. Kim *et al.*, "Development of 1MW inductive power transfer system for a high speed train," *IEEE Trans. Ind. Electron.*, vol. 62, no. 10, pp. 6242–6250, Oct. 2015.
[22] U. K. Madawala and D. J. Thrimawithana, "Modular-based inductive power transfer system for high-power applications," *IET Power Electron.*, vol. 5, pp. 1119–1126, 2013.
[23] H. R. Rahnamae, D. J. Thrimawithana, and U. K. Madawala, "MOSFET based multilevel converter for IPT systems," in *Proc. 2014 IEEE Int. Conf. Ind. Technol.*, 2014, pp. 295–300.
[24] H. R. Rahnamaee, U. K. Madawala, and D. J. Thrimawithana, "A multi-level converter for high power-high frequency IPT systems," in *Proc. IEEE 5th Int. Symp. Power Electron. Distrib. Gener. Syst.*, 2014, pp. 1–6.
[25] B. X. Nguyen, D. M. Vilathgamuwa, G. Foo, A. Ong, P. K. Sampathand, and U. K. Madawala, "Cascaded multilevel converter based bidirectional inductive power transfer (BIPT) system," in *Proc. Int. Power Electron. Conf.*, May 2014, pp. 2722–2728.
[26] H. Hao, G. A. Covic, and J. T. Boys, "A parallel topology for inductive power transfer power supplies," *IEEE Trans. Power Electron.*, vol. 29, no. 3, pp. 1140–1151, Mar. 2014.
[27] R. Johari, J. V. Krogmeier, and D. J. Love, "Analysis and practical considerations in implementing multiple transmitters for wireless power transfer via coupled magnetic resonance," *IEEE Trans. Ind. Electron.*, vol. 61, no. 4, pp. 1774–1783, Apr. 2014.
[28] D. Ahn and S. Hong, "Effect of coupling between multiple transmitters or multiple receivers on wireless power transfer," *IEEE Trans. Ind. Electron.*, vol. 60, no. 7, pp. 2602–2613, Jul. 2013.
[29] G. H. Sarma, G. Nitin, K. Mehta, and A. Bhattacharjee, "Reliability studies on high current power modules with parallel mosfets," in *Proc. Eur. Microelectron. Packag. Conf.*, 2009, pp. 1–7.
[30] J. A. Moreno-Cadenas, L. González-Carabarín, and F. Gómez-Castañeda, "Floating-gate MOSFET parallel analog network for assignment problems," in *Proc. 2010 7th Int. Conf. Electr. Eng. Comput. Sci. Autom. Control*, 2010, pp. 556–559.
[31] P. D. Smith, M. Kucic, and P. Hasler, "Accurate programming of analog floating-gate arrays," in *Proc. IEEE Int. Symp. Circuits Syst.*, 2002, pp. V-489–V-492.
[32] Y. Zhong, N. M. Roscoe, D. Holliday, and S. J. Finney, "MMC with parallel-connected MOSFETs for LVDC distribution networks," in *Proc. 8th IET Int. Conf. Power Electron., Mach. Drives*, 2016, pp. 1–6.
[33] J. Acero, C. Carretero, Ó. Lucía, R. Alonso, and J. M. Burdío, "Mutual impedance of small ring-type coils for multiwinding induction heating appliances," *IEEE Trans. Power Electron.*, vol. 28, no. 2, pp. 1025–1035, Feb. 2013.
[34] H. P. Ngoc, H. Fujita, K. Ozaki, and N. Uchida, "Phase angle control of high-frequency resonant currents in a multiple inverter system for zone-control induction heating," *IEEE Trans . Power Electron.*, vol. 26, no. 11, pp. 3357–3366, Nov. 2011.
[35] Y. Li, R. Mai, L. Lu, and Z. He, "Active and reactive currents decomposition-based control of angle and magnitude of current for a parallel multiinverter IPT system," *IEEE Trans. Power Electron.*, vol. 32, no. 2, pp. 1602–1614, Feb. 2017.
[36] S. Li, W. Li, J. Deng, T. D. Nguyen, and C. C. Mi, "A double-sided LCC compensation network and its tuning method for wireless power transfer," *IEEE Trans. Veh. Technol.*, vol. 64, no. 6, pp. 2261–2273, Jun. 2015.
[37] A. P. Hu, "Selected resonant converters for IPT power supplies," Ph.D. dissertation, Univ. Auckland, Auckland, New Zealand, 2001.
[38] Y. Song, U. K. Madawala, and A. P. Hu, "Cross coupling effects of polyphase bi-directional inductive power transfer systems used for EV charging," in *Proc. 2015 IEEE 2nd Int. Future Energy Electron. Conf.*, 2015, pp. 1–7.
[39] M. L. G. Kissin, J. T. Boys, and G. A. Covic, "Interphase mutual inductance in polyphase inductive power transfer systems," *IEEE Trans. Ind. Electron.*, vol. 56, no. 7, pp. 2393–2400, Jul. 2009.
[40] Z. Ye, P. K. Jain, and P. C. Sen, "Circulating current minimization in high-frequency AC power distribution architecture with multiple inverter modules operated in parallel," *IEEE Trans. Ind. Electron.*, vol. 54, no. 5, pp. 2673–2687, Oct. 2007.
[41] Nordic Semiconductor. nRF24L01+Datasheet, 2013. [Online]. Available: http://www.nordicsemi.com/eng/Products/2.4GHz-RF/nRF24L01P.

Yong Li (S'15) received the B.Sc. degree in electrical engineering, in 2013, from the Southwest Jiaotong University, Chengdu, China, where he is currently working toward the Ph.D. degree in electrical engineering.

His main research interests include wireless power transfer and resonant converters.

Ruikun Mai (M'14) received the B.Sc. and Ph.D. degrees in electrical engineering from the Southwest Jiaotong University, Chengdu, China, in 2004 and 2010, respectively.

Currently, he is an Associate Professor in the College of Electrical Engineering, Southwest Jiaotong University. His research interests include wireless power transfer and its application in railway systems, power system stability, and control.

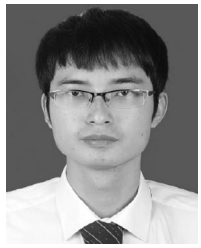

Liwen Lu received the B.Sc. degree in electrical engineering, in 2014, from the Southwest Jiaotong University, Chengdu, China, where he is currently working toward the M.Sc. degree in electrical engineering.

He is also with NR Electric Co. Ltd., Nanjing, China. His main research interests include control and protection of the power system, voltage source converter based high voltage direct current, and wireless power transfer.

Tianren Lin received the B.Sc. degree in electrical engineering, in 2015, from the Southwest Jiaotong University, Chengdu, China, where he is currently working toward the M.Sc. degree in electrical engineering.

His main research interest focuses on wireless power transfer.

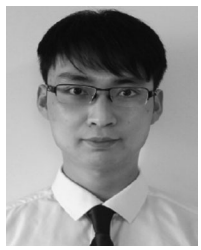

Yeran Liu (S'17) received the B.Sc. degree in electrical engineering from the School of Electrical Engineering, Southwest Jiaotong University E'mei Campus, E'mei, China, in 2015. Currently, he is working toward the Ph.D. degree in the School of Electrical Engineering, Southwest Jiaotong University, Chengdu, China.

His main research interest focuses on wireless power transfer.

Zhengyou He (M'10–SM'13) received the B.Sc. and M. Sc. degrees in computational mechanics from Chongqing University, Chongqing, China, in 1992 and 1995, respectively, and the Ph.D. degree in electrical engineering from the Southwest Jiaotong University, Chengdu, China, in 2001.

Currently, he is a Professor in the College of Electrical Engineering, Southwest Jiaotong University. His research interests include signal process and information theory applied to electrical power system, and application of wavelet transforms in power system.